J. Fluid Mech. (2013), *vol.* 732, *pp.* 660–686. © Cambridge University Press 2013
doi:10.1017/jfm.2013.425

Steady gravity waves due to a submerged source

Christopher J. Lustri[1],† **and S. Jonathan Chapman**[2]

[1]School of Mathematics and Statistics, University of Sydney, Sydney, NSW 2006, Australia

[2]Oxford Center for Industrial and Applied Mathematics, Mathematical Institute, University of Oxford, Oxford OX1 3LB, UK

(Received 12 June 2013; revised 12 June 2013; accepted 8 August 2013; first published online 12 September 2013)

In the low-Froude-number limit, free-surface gravity waves caused by flow past a submerged obstacle have amplitude that is exponentially small. Consequently, these cannot be represented using an asymptotic series expansion. Steady linearized flow past a submerged source is considered, and exponential asymptotic methods are applied to determine the behaviour of the free-surface gravity waves. The free surface is found to contain longitudinal and transverse waves that switch on rapidly across curves known as Stokes lines on the free surface. The longitudinal waves are present everywhere downstream of the singularity, while the transverse waves are restricted to two downstream wedges. As the depth of the source approaches the surface, the familiar Kelvin-wedge wave behaviour is recovered.

Key words: surface gravity waves, waves/free-surface flows

1. Introduction

1.1. *Background*

The earliest work on surface waves generated by flow past a submerged obstacle was that of Lamb (1879), in which the obstacle was considered to be a cylinder of infinite lateral extent, having radius small compared to its submergence depth. Later studies, such as those of Havelock (1917, 1919, 1931, 1932, 1949), considered surface waves produced by the flow past a range of different submerged obstacles. In these and almost all subsequent work, the obstacle is taken to be small, so that the disturbance to the stream is small and the free-surface condition can be linearized. This amounts to finding the flow over a point source (the Green function) from which other flows may be constructed.

A number of integral expressions have been obtained as solutions to steady flow past submerged obstacles using Green functions in this way. Havelock (1932) formulated an integral expression by dividing the surface behaviour into separate near-field non-oscillatory and far-field oscillatory integral expressions; this formulation was later modified by Lunde (1951). Alternative integral expressions of this Green function were found by Peters (1949) and implicitly by Michell (1898). Noblesse (1981, 1982) demonstrated that each of these integral expressions, as well as a number of others, could be obtained directly from the double Fourier inversion integral methods using

† Email address for correspondence: c.lustri@maths.usyd.edu.au

https://doi.org/10.1017/jfm.2013.425 Published online by Cambridge University Press

different transformations. Many of these results, as well as several alternative Green function expressions, are given by Wehausen & Laitone (1960).

More recently, Liu & Tao (2001) adapted the expression given by Wehausen & Laitone (1960) for surface wave behaviour to obtain an integral expression for the behaviour of unsteady flow past a submerged obstacle. Ockendon & Wilmott (1986) applied matched asymptotic expansions to determine the surface behaviour of inviscid flow past a submerged body in infinite depth.

Another large body of work on free-surface waves concerns the waves generated by flow past a ship hull. The most significant of these is that of Kelvin (1887), who famously found that gravity waves are present downstream from the ship, and that they are restricted to a wedge-shaped region known as a 'Kelvin wedge', contained within an angle of approximately 19.5° to the direction of motion. Ursell (1960) found that flow behaviour on the cusp lines bounding the Kelvin wedge is given in terms of Airy functions, while Akylas (1987) investigated the form of the unsteady nonlinear behaviour near the cusp lines.

Here we will be concerned with the low-Froude-number limit, where the Froude number represents the ratio of inertial to gravitational force, defined in (2.4). This limit has been explored in several previous studies, particularly in the context of ship hydrodynamics, using asymptotic power series methods. Ogilvie (1968) considered the problem of a submerged two-dimensional object, noting that the asymptotic series in powers of the Froude number failed to produce wave behaviour on the calculated free surface. Dagan & Tulin (1972) considered the wave resistance of a blunt bow, also obtaining waveless solutions up to second-order in the Froude number. Vanden-Broeck, Schwartz & Tuck (1978) investigated several free-surface flow problems in this limit, using Padé approximant representations of the solutions in order to obtain discontinuous free-surface profiles. In more general problems from fluid dynamics, Peregrine (1972) considered the low-Froude-number problem of flow due to a line source or sink, finding the solution to be waveless up to fourth-order. The wavelessness of the free surface in these expansions is now known as the low-speed paradox.

For surface piercing objects such as ships, however, the situation is quite different. Keller (1979) was able to calculate the free-surface wave behaviour of flow past a ship using geometric ray theory, which is applicable when the disturbance is on the surface of the flow. This study considered the problem of flow past thin ships, as well as more general ship hulls, and found that the surface contained downstream gravity waves, located within the familiar Kelvin wedge. This study complemented earlier work by Baba (1976), and Maruo & Suzuki (1977), who considered the problem of flow past streamlined ships. The problem of flow past thin ships is of particular interest in the current investigation, which may be thought of as an extension of this analysis to the case when the singularities associated with the thin ship are submerged.

Allowing the flow obstruction to be submerged produces a substantially more complicated problem. The geometric ray tracing applied by Keller is no longer applicable, and applying asymptotic series methods directly fails to capture the wave behaviour, as in the studies listed above. In general, gravity waves past a submerged obstacle cannot be captured by an asymptotic power series in the Froude number, as they are exponentially small in the low-Froude-number limit, and hence smaller than any power of the Froude number. We may see the reason for this behaviour by considering a steady train of two-dimensional surface waves on deep water. Following Vanden-Broeck *et al.* (1978), we note that the wavelength of linearized free-surface waves on a flow with speed U and a representative length scale L is related to the

https://doi.org/10.1017/jfm.2013.425 Published online by Cambridge University Press

Froude number, defined in (2.4), by

$$\lambda/L = 2\pi U^2/gL = 2\pi F^2. \tag{1.1}$$

We therefore expect the free-surface position to be a sinusoidal wave, and hence that the fluid potential on the surface can be given to within an arbitrary phase shift by

$$\phi = \varphi(y)\sin(2\pi x/\lambda) = \varphi(y)\sin(x/F^2), \tag{1.2}$$

where all distances have been scaled by L. Noting that the fluid potential ϕ must satisfy Laplace's equation (2.1), we find that

$$\varphi(y) = C_1\exp(y/F^2) + C_2\exp(-y/F^2), \tag{1.3}$$

where C_i denote arbitrary constants. Rejecting the possibility of waves that are exponentially large as the Froude number decays as physically unreasonable, we conclude that any steady wavetrain present on a free surface must be exponentially small as $F \to 0$.

Fortunately, a set of methods known as exponential asymptotic techniques, such as those described in Berry & Howls (1990), Berry (1991), Olde Daalhuis *et al.* (1995) and Chapman *et al.* (1998), have been developed for the purpose of calculating such behaviour. More general introductions to exponential asymptotic methods are found in Paris & Wood (1995), Jones (1997) and Boyd (1998), while comprehensive treatments are given by Segur *et al.* (1991) and Boyd (2005).

Exponential asymptotic methods were first applied to resolve the low-speed paradox by Chapman & Vanden-Broeck (2006). That investigation considered the problem of gravity waves on free-surface flow over a general submerged obstacle in the low-Froude-number limit. The authors applied hodograph mapping methods, similar to those used in Forbes & Schwartz (1982), to map from the physical flow path to an upper-half complex plane. In the mapped system, the equations governing the system were formulated as a Cauchy integral equation in the body of the flow, and a differential equation governing the free-surface behaviour. The free surface was analytically continued, so that the free-surface behaviour could be found using the exponential asymptotic methodology developed in Olde Daalhuis *et al.* (1995) and Chapman *et al.* (1998). The authors determined that exponentially small gravity waves are present downstream from the obstacle, and that these waves are switched on rapidly across curves on the complexified free surface known as 'Stokes lines', which will be discussed in § 1.2.

Following this work, Lustri, McCue & Binder (2012) applied exponential asymptotic methods to determine the low-Froude-number behaviour of waves downstream from a submerged bump or trench in two dimensions, as well as to show the existence of trapped wave configurations in both cases. Trinh, Chapman & Vanden-Broeck (2011) considered the problem of flow past a surface-piercing hull, demonstrating that waveless surfaces are not possible for hulls with one corner. Lustri, McCue & Chapman (2013) determined the behaviour of far-field gravity waves caused by a submerged source in a channel of finite depth.

Each of the previous exponential asymptotic investigations into the behaviour of free-surface gravity waves in the low-Froude-number limit takes place in two dimensions, and is formulated using the complex variable methods described in Chapman & Vanden-Broeck (2006). In the present study, we instead consider the problem of infinite-depth flow past a point source in three dimensions. In three dimensions, we can longer apply the complex mapping techniques used in the

https://doi.org/10.1017/jfm.2013.425 Published online by Cambridge University Press

previously studied two-dimensional problems. Instead, we will consider the strength of the submerged source to be weak, and linearize the problem in this parameter, fixing the position of the boundary. We subsequently apply exponential asymptotic techniques directly to the governing flow equations, without applying any mappings to the system.

As previously noted, in the limit that the depth of the source tends to zero, and hence that the singularity moves onto the surface of the flow, this problem tends to the thin-ship wave problem investigated by Keller (1979) using geometric ray theory. Consequently, the problem of a submerged source or obstacle may be thought of as an extension to this work which incorporates the theory of complex rays (see Chapman, Lawry & Tew 1999) when the source is not located on the surface of the flow. In this case, the singularity is now located on the complexified free surface, and it is this singular behaviour that generates the downstream surface waves.

Finally, we note that exponential asymptotic methods have been used to consider free-surface fluid flow problems in other limits. Chapman & Vanden-Broeck (2002) applied exponential asymptotic methods to determine the behaviour of upstream capillary waves for flow over a submerged obstacle in the low-Bond-number limit, while the more complicated case of gravity–capillary waves with low Froude number and Bond number was investigated by Trinh & Chapman (2013*a*,*b*). The behaviour of weakly non-local solitary waves was investigated by Grimshaw & Joshi (1995) and Grimshaw (2011), as well as by Trinh (2011) using methods similar to those presented here. Keller & Ward (1996) considered slow flow past a cylinder with small Reynolds number, using exponential asymptotics to determine the drag on the cylinder, and local asymmetry of the flow (also discussed in Ward & Kropinski 2011).

1.2. *Methodology*

It was Stokes (1864) who first observed that a function containing multiple exponentials in the complex plane can contain curves along which the behaviour of the subdominant exponential apparently changes discontinuously. These curves are known as Stokes lines. Using exponential asymptotic methods, Berry (1988) was able to investigate this switching behaviour, known as the Stokes phenomenon, finding that the variation was smooth, but rapid, occurring in the neighbourhood of the Stokes line. This Stokes switching behaviour will play an important role in the present investigation. We will make extensive use of the technique developed by Olde Daalhuis *et al.* (1995) and extended by Chapman *et al.* (1998) for investigating it.

The first step in this technique is to express the solution as an asymptotic power series, such as

$$f(x;\epsilon) \sim \sum_{n=0}^{\infty} \epsilon^n a_n(x) \quad \text{as } \epsilon \to 0. \tag{1.4}$$

Because we are considering a singular perturbation problem, the series will be divergent. The approximation error can be minimized by truncating the series optimally. To find the optimal truncation point, we follow the commonly used strategy described by Boyd (1999), in which the series is truncated at its smallest term. Boyd notes that this is not a universal law, and indeed that counter-examples may be constructed. However, it has been proven true for several classes of asymptotic series (for example, Costin & Kruskal 1996, 1999; Olde Daalhuis 1998), and will be sufficient for use in this investigation.

https://doi.org/10.1017/jfm.2013.425 Published online by Cambridge University Press

Unfortunately, determining the smallest term in the series, and consequently the optimal truncation point, is challenging. The method described by Olde Daalhuis *et al.* (1995) requires a general form for the asymptotic series coefficients $a_n(x)$. While such a form may be obtained for the solutions to some classes of problems, such as linear ordinary differential equations, in many other problems the series terms become algebraically intractable after even a small number of terms.

To overcome this difficulty, Chapman *et al.* (1998) observed that the optimal truncation point tends to become large in the asymptotic limit. Hence, knowledge of the behaviour of the late-order terms of the series (that is, the form of a_n in the limit that $n \to \infty$) is sufficient to truncate the asymptotic series optimally. Fortunately, the late-order terms of an asymptotic series often behave in predictable fashion, even if the general form of the series terms is too complicated to be found explicitly.

In singular perturbation problems, Dingle (1973) noted that successive terms in the asymptotic series expansion are obtained by repeated differentiation of an earlier term in the series. Hence, the late-order terms of the resultant asymptotic series diverge as the ratio between a factorial and the increasing power of a function χ, such as

$$a_n \sim \frac{A\Gamma(n+\gamma)}{\chi^{n+\gamma}} \quad \text{as } n \to \infty, \tag{1.5}$$

where Γ is the gamma function defined in Abramowitz & Stegun (1972), and A, γ and χ are functions that do not depend on n.

Chapman *et al.* (1998) therefore propose a factorial-over-power ansatz for the late-order terms, (1.5). They conclude that the correct late-term behaviour may be represented as the sum of these ansatz expressions, each associated with a different singularity of the leading-order solution. The global behaviour of the functions A, γ and χ may be found by substituting this ansatz directly into the equations governing the asymptotic series terms, and then matching to the local behaviour in the neighbourhood of the singularity under consideration (in particular χ will be zero at the singularity).

Furthermore, they note that the late-order term behaviour given in (1.5) is related to applying a WKB ansatz of the form $Ae^{-\chi/\epsilon}$ to the equation for f linearized about the truncated expansion. Consequently, the behaviour of χ, or the 'singulant', will play an important role in understanding the Stokes line behaviour. Recalling that Stokes switching will occur when the switching exponential is maximally subdominant, we recognize that this will occur when the singulant is purely real and positive. This is therefore a convenient condition to determine the possible location of Stokes lines, as observed by Dingle (1973).

Once the form of the late-order terms is established, we may determine the optimal truncation point by finding the point at which terms in the series change from decreasing to increasing. To do so, we find the truncation value at which the ratio of consecutive terms is equal to one. Truncating the series at this point gives

$$f(x;\epsilon) = \sum_{n=0}^{N-1} \epsilon^n a_n(x) + R_N, \tag{1.6}$$

where $N(x;\epsilon)$ is the optimal truncation point, and R_N is the now exponentially small remainder term.

Now Olde Daalhuis *et al.* (1995) substitute the truncated series expression back into the original problem, obtaining an equation for the exponentially small remainder term itself. The positions of Stokes lines are found by determining the curves along which

https://doi.org/10.1017/jfm.2013.425 Published online by Cambridge University Press

the remainder term varies rapidly, and the switching behaviour of this remainder is found by solving the remainder equation in the neighbourhood of these Stokes lines.

A key step in the method just described is the identification of the singularities in the leading-order solution, since these generate the divergent terms such as (1.5) and their associated Stokes lines. For the free-boundary problems considered here, x represents position on the free surface.

In the investigation of flow over submerged disturbances, the flow behaviour typically contains no singularities on the free boundary itself; however, there are singularities present when the boundary is analytically continued. In the problem under consideration here, we will see that the singularities that govern the Stokes line behaviour are found by analytically continuing the free surface into the complex plane.

We make one final remark before we proceed to apply these techniques to our free-surface problem. The exponential asymptotic methodology of Olde Daalhuis *et al.* (1995) and Chapman *et al.* (1998) was developed for investigating ordinary differential equations. Because our free surface is two-dimensional, we will require the extension of these techniques to partial differential equations which was developed by Chapman & Mortimer (2005).

Initially, the method is identical, with the Stokes switching being found by expanding the solution as an asymptotic power series, applying an ansatz to the late-order terms, optimally truncating the series, and then determining the behaviour of the exponentially small remainder R_N in the neighbourhood of the Stokes line. However, in some partial differential equations (and indeed, in higher-order differential equations), further Stokes switching may occur. If the remainder is expanded as

$$R_N \sim \mathrm{e}^{-\chi/\epsilon} \sum_{n=0}^{\infty} \epsilon^n R_N^{(n)} \quad \text{as } \epsilon \to 0, \tag{1.7}$$

then again applying the method of Olde Daalhuis *et al.* (1995) and Chapman *et al.* (1998), we can truncate optimally, giving

$$R_N = \mathrm{e}^{-\chi/\epsilon} \sum_{n=0}^{M-1} \epsilon^n R_N^{(n)} + S_M, \tag{1.8}$$

where S_M is the new (doubly) exponentially subdominant remainder term. Obviously, it is possible to conceive of problems in which the remainder S_M may be expanded as another exponentially subdominant divergent asymptotic series, and so on. Hence, we find that a hierarchy of increasingly exponentially subdominant late-order contributions may be present in the asymptotic expression. The relative size of these exponentials may change depending on where we are on the free surface.

2. Formulation

Consider the steady-state problem of uniform flow past a submerged point source in three dimensions. We suppose that the strength of the source is small so that the problem may be linearized.

2.1. *Full problem*

We consider a three-dimensional incompressible irrotational inviscid free-surface flow of infinite depth with a submerged point source at depth H and upstream flow velocity U. We normalize the fluid velocity with U and distance with an unspecified length L, giving non-dimensionalized source depth $h = H/L$, shown schematically in figure 1.

https://doi.org/10.1017/jfm.2013.425 Published online by Cambridge University Press

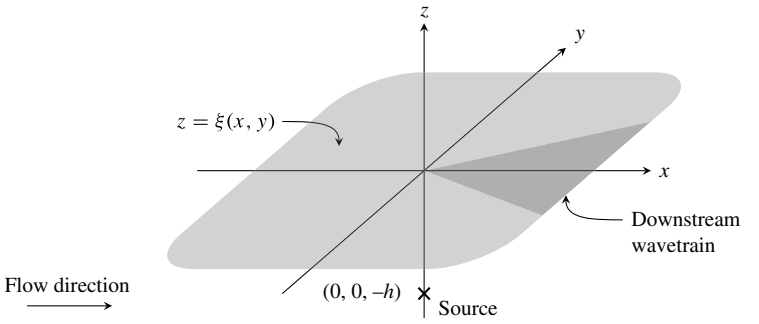


FIGURE 1. Prescribed fluid configuration for three-dimensional flow over a source. The shaded region represents the position of the free surface $\xi(x, y)$, and the cross represents the position of the source. The flow region lies below the free surface, and the mean flow is moving from left to right, with flow velocity U in the unscaled problem. A possible downstream wave region is illustrated in darker grey.

The natural choice for L is H, but we prefer to separate H and L so that we may later more easily take the limit $h \to 0$ to compare our results with those of Keller (1979).

Denoting the (non-dimensional) position of the free surface by $z = \xi(x, y)$, the (non-dimensional) velocity potential satisfies

$$\nabla^2\phi = 0, \quad -\infty < z < \xi(x, y), \tag{2.1}$$

with kinematic and dynamic boundary conditions

$$\xi_x\phi_x + \xi_y\phi_y = \phi_z, \quad z = \xi(x, y), \tag{2.2}$$

$$\tfrac{1}{2}\epsilon(|\nabla\phi|^2 - 1) + \xi = 0, \quad z = \xi(x, y), \tag{2.3}$$

where we have written $\epsilon = F^2$, where

$$F = \frac{U}{\sqrt{gL}} \tag{2.4}$$

is the Froude number, and g is the acceleration due to gravity. We will be concerned with the limit $0 < \epsilon \ll 1$. Since the flow is uniform in the far field, $\phi_x \to 1$ there, while at the source

$$\phi \sim \frac{\delta}{4\pi\sqrt{x^2 + y^2 + (z + h)^2}} \quad \text{as } (x, y, z) \to (0, 0, -h). \tag{2.5}$$

We will be concerned with the limit $0 < \delta \ll \epsilon$, so that the disturbance to the free stream is weak and the equations may be linearized in δ.

Finally, we require a radiation condition which states that any waves generated must have an outgoing group velocity. In this case, this means that the surface gravity waves may only be present at infinity downstream of the source.

2.2. *Linearization*

We linearize about uniform flow by setting

$$\phi = x + \delta\overline{\phi}, \quad \xi = \delta\overline{\xi}, \tag{2.6}$$

https://doi.org/10.1017/jfm.2013.425 Published online by Cambridge University Press

to give, at leading-order in δ,

$$\nabla^2\overline{\phi} = 0, \quad -\infty < z < 0, \tag{2.7}$$

$$\overline{\phi}_z - \overline{\xi}_x = 0, \quad z = 0, \tag{2.8}$$

$$\epsilon\overline{\phi}_x + \overline{\xi} = 0, \quad z = 0, \tag{2.9}$$

where the boundary conditions are now applied on the fixed surface $z = 0$. The far-field conditions imply that $\overline{\phi} \to 0$ as $x^2 + y^2 + z^2 \to \infty$, while near the source

$$\overline{\phi} \sim \frac{1}{4\pi\sqrt{x^2 + y^2 + (z+h)^2}} \quad \text{as } (x, y, z) \to (0, 0, -h). \tag{2.10}$$

With the addition of a radiation condition, specifying that gravity waves may only propagate downstream, the system described in (2.7)–(2.10) completely specifies the linearized version of the three-dimensional problem shown in figure 1.

We analytically continue the free surface such that $x, y \in \mathbb{C}$, with the free surface still satisfying $z = 0$. This does not change the form of (2.7)–(2.10), but it does mean that the two-dimensional physical free surface is now a subset of a four-dimensional complexified free surface.

2.3. *Series expression*

Following the approach of Chapman & Vanden-Broeck (2006), we first expand the fluid potential and free-surface position as a power series in ϵ,

$$\overline{\phi} \sim \sum_{n=0}^{\infty} \epsilon^n \phi^{(n)}, \quad \overline{\xi} \sim \sum_{n=0}^{\infty} \epsilon^n \xi^{(n)}, \tag{2.11}$$

to give for $n \geqslant 0$

$$\nabla^2\phi^{(n)} = 0, \quad -\infty < z < 0, \tag{2.12}$$

$$\phi^{(n)}_z - \xi^{(n)}_x = 0, \quad z = 0, \tag{2.13}$$

$$\phi^{(n-1)}_x + \xi^{(n)} = 0, \quad z = 0, \tag{2.14}$$

with the convention that $\phi^{(-1)} = 0$. The far-field behaviour tends to zero at all orders of n, and the singularity condition (2.10) is applied to the leading-order expression, giving

$$\phi^{(0)} \sim \frac{1}{4\pi\sqrt{x^2 + y^2 + (z+h)^2}} \quad \text{as } (x, y, z) \to (0, 0, -h). \tag{2.15}$$

The leading-order solution is simply

$$\phi^{(0)} = \frac{1}{4\pi\sqrt{x^2 + y^2 + (z+h)^2}} + \frac{1}{4\pi\sqrt{x^2 + y^2 + (z-h)^2}}, \quad \xi^{(0)} = 0. \tag{2.16}$$

From (2.14), this gives

$$\xi^{(1)} = \frac{x}{2\pi(x^2 + y^2 + h^2)^{3/2}}. \tag{2.17}$$

Through repeated iteration of (2.13)–(2.14), we find that the position of singularities in subsequent terms of the series (2.11) remains constant, while the power of the singularity increases at each order, as we expect for such singular perturbation problems (see Chapman & Vanden-Broeck 2006).

https://doi.org/10.1017/jfm.2013.425 Published online by Cambridge University Press

3. Late-order terms

In order to optimally truncate the asymptotic series prescribed in (2.11), we must determine the form of the late-order terms. To accomplish this, we make the factorial-over-power ansatz (see Chapman *et al.* 1998)

$$\phi^{(n)} \sim \frac{\Phi(x,y,z)\Gamma(n+\gamma)}{\chi(x,y,z)^{n+\gamma}}, \quad \xi^{(n)} \sim \frac{\Xi(x,y)\Gamma(n+\gamma)}{\chi(x,y,0)^{n+\gamma}}, \quad \text{as } n \to \infty, \tag{3.1}$$

where γ is a constant. As discussed in § 1.2, the function χ that is raised to the power of n is known as the 'singulant'. For (3.1) to be consistent with (2.16) we require that the singulant satisfies

$$\chi = 0 \quad \text{on } x^2 + y^2 + (z \pm h)^2 = 0, \tag{3.2}$$

where the sign chosen depends upon which of the two singularities is being considered. For complex values of x, y and z, this defines a four-dimensional hypersurface. Irrespective of which singularity is under consideration, this hypersurface intersects the four-dimensional complexified free surface on the two-dimensional hypersurface satisfying $x^2 + y^2 + h^2 = 0$.

It is important to note that the expression for $\xi^{(n)}$ is restricted to $z = 0$, as it describes the free-surface position. This does not pose a problem for the subsequent analysis, but does ensure that care must be taken at each stage to determine whether we are considering the full flow region, or just the free surface.

3.1. *Calculating the singulant*

Applying the ansatz expressions in (3.1) to the governing equation (2.12) and taking the first two orders as $n \to \infty$ gives

$$\chi_x^2 + \chi_y^2 + \chi_z^2 = 0, \tag{3.3}$$

$$2\Phi_x\chi_x + 2\Phi_y\chi_y + 2\Phi_z\chi_z = -(\chi_{xx} + \chi_{yy} + \chi_{zz}), \tag{3.4}$$

while the boundary conditions on $z = 0$ become, to leading-order,

$$-\chi_z\Phi + \chi_x\Xi = 0, \tag{3.5}$$

$$-\chi_x\Phi + \Xi = 0. \tag{3.6}$$

The system in (3.5)–(3.6) has non-zero solutions when $\chi_x^2 = \chi_z$. Combining this result with (3.3) evaluated on $z = 0$ gives an eikonal equation for χ on the free surface,

$$\chi_x^4 + \chi_x^2 + \chi_y^2 = 0. \tag{3.7}$$

The eikonal equation (3.7) is identical to that obtained in Keller (1979) for the case of a surface disturbance, given there in terms of the wave vector $\boldsymbol{k} = \nabla s$, where s is the phase function of the surface waves and is equivalent to $\mathrm{i}\chi$ in our notation.

Here, however, because the singularity lies below the fluid surface, we must solve (3.7) for complex x and y with the boundary condition

$$\chi = 0 \quad \text{on } x^2 + y^2 + h^2 = 0. \tag{3.8}$$

Parameterizing (3.8) as

$$x_0 = s, \quad y_0 = \pm\mathrm{i}\sqrt{s^2 + h^2}, \quad \chi_0 = 0, \tag{3.9}$$

and solving (3.7) using Charpit's method (see Ockendon *et al.* 1999) gives

$$\chi = \frac{2h^4 u}{s^4}, \tag{3.10}$$

https://doi.org/10.1017/jfm.2013.425 Published online by Cambridge University Press

where u is one of

$$u = \pm \frac{h^3(s-x)}{s(2h^2+s^2)} \tag{3.11}$$

and s is any one of the four solutions to

$$\left(x^2+y^2\right)s^4 + 4xh^2s^3 + \left(h^2x^2+4h^2y^2+4h^4\right)s^2 + 4h^4xs + \left(4y^2h^4+4h^6\right) = 0. \tag{3.12}$$

Consequently, we have obtained a set of possible expressions for the singulant χ (that is, the expression raised to the power of n in the late-order terms (3.1)). As discussed in § 1.2, the singulant will also appear in the exponent of the associated exponentially small free-surface behaviour, and hence determines the position of the Stokes lines on the free surface.

Equations (3.10)–(3.12) give eight possible expressions for the singulant (corresponding to the choice of sign in (3.10) and the four solutions to (3.12)). These therefore give eight possible sets of late-order behaviour in the problem. We will only consider four of these expressions, since the other four would produce exponentially large free-surface waves in the far field and may therefore be discarded on physical grounds.

Plots illustrating the behaviour of the remaining singulant terms are presented in figure 2 for $h = 1$. We have labelled the singulants according to their behaviour on the physical free surface, where χ_{L1} and χ_{L2} are associated with longitudinal waves on the free surface, while χ_{T1} and χ_{T2} are associated with transverse waves; the reason for this terminology will be shown in figure 8.

Each of these expressions satisfies $\mathrm{Im}(\chi) = 0$ along the curve $x = 0$, irrespective of h; however, only the behaviour illustrated in figure 2(*a*) satisfies $\mathrm{Re}(\chi) > 0$ along this curve. Recalling from § 1.2 that Stokes switching requires both of these conditions to hold, we determine that there is a Stokes line associated with $\chi_{L1,2}$ along this curve, but not one associated with $\chi_{T1,2}$. Knowing that any contribution switched across Stokes lines must only be present in the downstream far field due to the radiation condition, we therefore conclude that the free surface contains an exponentially small downstream contribution associated with $\chi_{L1,2}$ which switches on across the curve $x = 0$.

3.2. *Calculating the prefactor*

In order to obtain a complete expression for the late-order terms (3.1), we require an expression for the prefactors, Φ and Ξ. To find the prefactor equation, we consider the next order in (2.13)–(2.14) as $n \to \infty$. From (3.6), we obtain

$$\Xi = \chi_x \Phi. \tag{3.13}$$

Expanding the prefactors in the form of a power series in n as $n \to \infty$,

$$\Phi = \Phi_0 + \frac{1}{n}\Phi_1 + \cdots, \quad \Xi = \Xi_0 + \frac{1}{n}\Xi_1 + \cdots, \tag{3.14}$$

and applying the late-order ansatz to (3.3)–(3.5) now gives

$$-\chi_z\Phi_1 + \Phi_{0,z} + \chi_x\Xi_1 - \Xi_{0,x} = 0, \tag{3.15a}$$

$$-\chi_x\Phi_1 + \Phi_{0,x} + \Xi_1 = 0. \tag{3.15b}$$

Recalling that $\chi_z = \chi_x^2$, we multiply (3.15*b*) by χ_x. Subtracting one equation from the other then eliminates all terms containing Φ_1 and Ξ_1, leaving

$$\chi_x\Phi_{0,x} - \Phi_{0,z} + \Xi_{0,x} = 0. \tag{3.16}$$

https://doi.org/10.1017/jfm.2013.425 Published online by Cambridge University Press

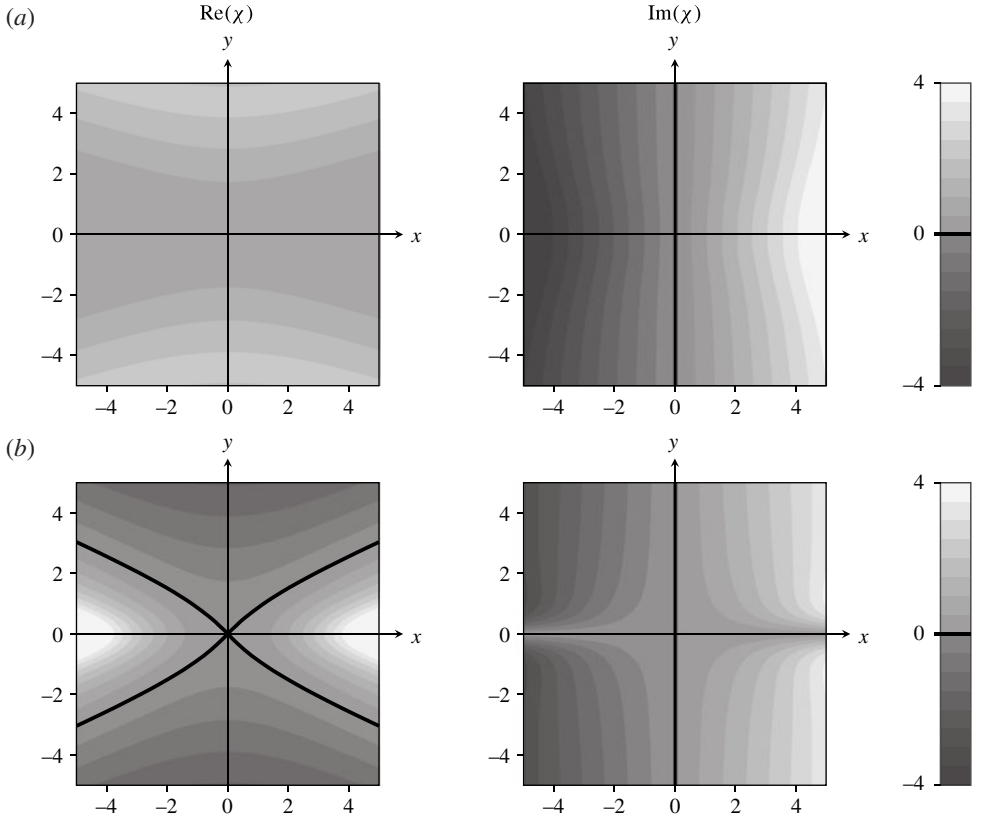


FIGURE 2. Singulants obtained by solving (3.7) with boundary data (3.8): (*a*) behaviour of χ_{L1}; (*b*) behaviour of χ_{T1}. The behaviour of χ_{L2} and χ_{T2} are given by the complex conjugates of these solutions. We note that $\mathrm{Re}(\chi_{L1}) > 0$ over the entire domain.

This equation must be solved together with (3.6). Since we are interested here in the leading-order behaviour of the prefactor, for ease of notation we now omit the subscripts and denote Ξ_0 by Ξ and Φ_0 by Φ.

Since we are interested mainly in the behaviour on the free surface, we use (3.4) to eliminate Φ_z, to give an equation on $z = 0$ only containing derivatives in x and y, namely

$$(4\chi_x^3 + 2\chi_x)\Phi_x + 2\chi_y\Phi_y = -(\chi_{xx} + \chi_{yy} + 6\chi_x^2\chi_{xx})\Phi. \tag{3.17}$$

This equation may be solved using the method of characteristics, giving the ray equations (with characteristic variable u) as

$$\frac{\mathrm{d}x}{\mathrm{d}u} = 4\chi_x^3 + 2\chi_x, \quad \frac{\mathrm{d}y}{\mathrm{d}u} = 2\chi_y, \quad \frac{\mathrm{d}\Phi}{\mathrm{d}u} = -(\chi_{xx} + \chi_{yy} + 6\chi_x^2\chi_{xx})\Phi. \tag{3.18}$$

The first two of these equations govern the ray paths, and are identical to the ray equations associated with (3.7). This allows (3.18) to be written in terms of the

https://doi.org/10.1017/jfm.2013.425 Published online by Cambridge University Press

associated Charpit variables, and solved to give

$$\Phi(s,u)=\Phi(s,0)\sqrt{\frac{s^4}{6hus^2+4h^3u+s^4}}. \tag{3.19}$$

Selecting the corresponding expressions for s and u in terms of x and y from (3.11) and (3.12) gives the solution in terms of the physical coordinates x and y. To find an expression for $\Phi(s,0)$, the behaviour of the system in the neighbourhood of $u=0$ must be computed and matched to this outer solution. The appropriate inner analysis is performed in appendix A, and gives

$$\Phi(s,0)=\frac{h^{1/2}}{4\pi s^{1/2}\sqrt{2\pi}}. \tag{3.20}$$

Finally, to find γ, we ensure that the strength of the singularity in the late-order behaviour $\phi^{(n)}$, given in (3.1) in the limit that $n\to 0$ is consistent with the leading-order behaviour $\phi^{(0)}$, which has strength $1/2$. This implies that near the singularity at $x^2+y^2+h^2=0$,

$$\frac{\Phi\Gamma(\gamma)}{\chi^\gamma}\to\frac{\alpha(x,y)}{(x^2+y^2+h^2)^{1/2}}, \tag{3.21}$$

where α is of order one in the limit. From (3.19), we see that the prefactor is also order one in this limit, while the local analysis near the singularity (A 1) showed that $1/\chi$ will be a singularity with strength one at $x^2+y^2+h^2=0$. Consequently, matching the order of the expressions in (3.21) gives $\gamma=1/2$.

We have therefore completely described the late-order terms given in (3.1), where (3.6) is used to determine the value of Ξ.

4. Stokes smoothing

The asymptotic series given in (2.11) may be truncated to give

$$\overline{\phi}=\sum_{n=0}^{N-1}\epsilon^n\phi^{(n)}+R^{(N)},\quad \overline{\xi}=\sum_{n=0}^{N-1}\epsilon^n\xi^{(n)}+S^{(N)}, \tag{4.1}$$

where N will be chosen in order to minimize the remainders $R^{(N)}$ and $S^{(N)}$. Applying this series expression to (2.7) gives

$$\nabla^2R^{(N)}=0, \tag{4.2}$$

while the boundary conditions (2.8)–(2.9) become on $z=0$

$$R_z^{(N)}-S_x^{(N)}=0, \tag{4.3}$$

$$\epsilon R_x^{(N)}+S^{(N)}=-\epsilon^N\phi_x^{(N-1)}, \tag{4.4}$$

having made use of the relationship in (2.14) and the fact that $\xi^{(0)}=0$. The homogeneous form of (4.2)–(4.4) is satisfied as $\epsilon\to 0$ by

$$R^{(N)}\sim\Phi\mathrm{e}^{-\chi/\epsilon},\quad S^{(N)}\sim\Xi\mathrm{e}^{-\chi/\epsilon}, \tag{4.5}$$

where χ is one of the singulants determined from (3.10)–(3.12).

We therefore set the remainder terms for the inhomogeneous problem to take the form

$$R^{(N)}=A(x,y,z)\Phi\mathrm{e}^{-\chi/\epsilon},\quad S^{(N)}=B(x,y)\Xi\mathrm{e}^{-\chi/\epsilon}, \tag{4.6}$$

https://doi.org/10.1017/jfm.2013.425 Published online by Cambridge University Press

where A and B are Stokes switching parameters. From (4.3), we see that $A = B$ on $z = 0$.

To determine the late-order term behaviour, we will require the first correction term for the prefactors, and we therefore set

$$\Phi = \Phi_0 + \epsilon\Phi_1 + \cdots, \quad \Xi = \Xi_0 + \epsilon\Xi_1 + \cdots. \tag{4.7}$$

Applying the remainder forms given in (4.6) to the boundary conditions, (4.3) and (4.4), gives after some rearrangement

$$-\chi_z A\Phi_1 + A\Phi_{0,z} + A_z\Phi_0 + \chi_x A\Xi_1 - A\Xi_{0,x} - A_x\Xi_0 = 0, \tag{4.8}$$

$$-\chi_x A\Phi_1 + A\Phi_{0,x} + A_x\Phi_0 + A\Xi_1 = -\epsilon^N \phi_x^{(N-1)} \mathrm{e}^{\chi/\epsilon}. \tag{4.9}$$

Combining these expressions, and making use of (3.16) to eliminate terms and (2.14) to simplify the right-hand side gives

$$A_z\Phi_0 - A_x\Xi_0 + \chi_x A_x\Phi_0 \sim \chi_x \epsilon^N \xi^{(N)} \mathrm{e}^{\chi/\epsilon}. \tag{4.10}$$

As only the leading-order prefactor behaviour appears in the final expression, we will no longer retain the subscripts. Applying the late-order ansatz gives

$$A_z\Phi - A_x\Xi + \chi_x A_x\Phi \sim \chi_x \epsilon^N \frac{\Xi\Gamma(N+1/2)}{\chi^{N+1/2}} \mathrm{e}^{\chi/\epsilon}. \tag{4.11}$$

Motivated by the homogeneous solution, we express the equation in terms of χ and y, and apply (3.13) to obtain

$$A_\chi = \epsilon^{N-1} \mathrm{e}^{\chi/\epsilon} \frac{\Gamma(N+1/2)}{\chi^{N+1/2}}. \tag{4.12}$$

The optimal truncation point is given by $N \sim |\chi|/\epsilon$ in the limit that $\epsilon \to 0$. We write $\chi = r\mathrm{e}^{\mathrm{i}\theta}$, with r and θ real so that $N = r/\epsilon + \alpha$, where α is necessary to make N an integer. Since N depends on r but not θ, we write

$$\frac{\partial}{\partial\chi} = -\frac{\mathrm{i}\mathrm{e}^{-\mathrm{i}\theta}}{r}\frac{\partial}{\partial\theta}. \tag{4.13}$$

Using Stirling's formula on the resultant expression gives

$$A_\theta \sim \frac{\mathrm{i}\sqrt{2\pi r}}{\epsilon} \exp\left(\frac{r}{\epsilon}\left(\mathrm{e}^{\mathrm{i}\theta} - 1\right) - \mathrm{i}\theta\left(\frac{r}{\epsilon} + \alpha - \frac{1}{2}\right)\right). \tag{4.14}$$

This variation is exponentially small, except in the neighbourhood of the Stokes line, given by $\theta = 0$, where it is algebraically large. To investigate the rapid change in A in the vicinity of the Stokes line, we set $\theta = \epsilon^{1/2}\hat{\theta}$, giving

$$A_{\hat{\theta}} \sim \mathrm{i}\sqrt{\frac{2\pi r}{\epsilon}} \mathrm{e}^{-r\hat{\theta}^2/2}, \tag{4.15}$$

so that

$$A \sim \mathrm{i}\sqrt{\frac{2\pi}{\epsilon}} \int_{-\infty}^{\theta\sqrt{r/\epsilon}} \mathrm{e}^{-t^2/2}\,\mathrm{d}t + C, \tag{4.16}$$

https://doi.org/10.1017/jfm.2013.425 Published online by Cambridge University Press

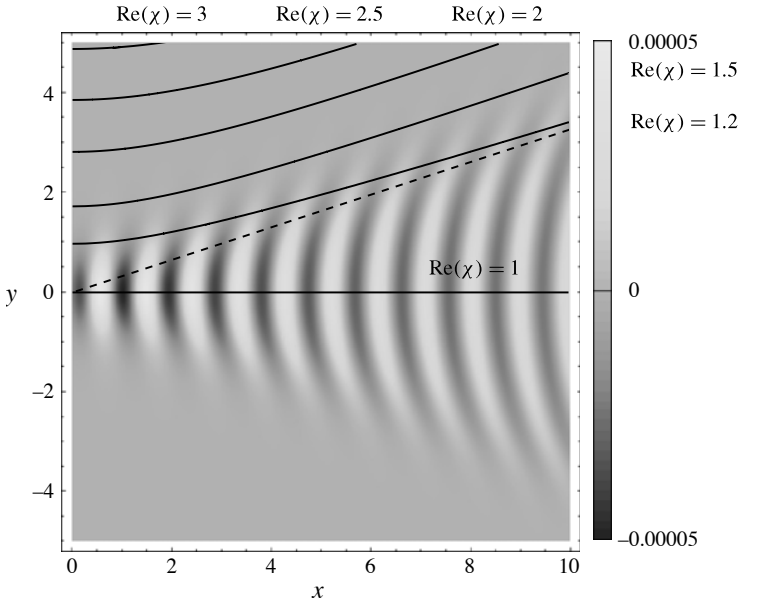


FIGURE 3. Exponentially small contribution to the free-surface behaviour with $\epsilon = 0.15$ and $h = 1$, given in (4.18). The waves switches on rapidly across the curve $x = 0$ and generates waves on the positive side of the Stokes line. These waves appear to be restricted to a wedge-shaped region of the domain, but are in fact present for all $x > 0$. In the regions of the surface that appear flat, the waves are simply exponentially small compared to the visible waves within the wedge. The thick contours illustrate the behaviour of $\mathrm{Re}(\chi_L)$, while the dashed line shows the Kelvin wedge. Identical contours are present in the lower-half-plane, although these have been omitted from the figure. These contours show that the exponential is almost constant within the Kelvin wedge, while decaying outside it.

where C is constant. Thus, as the Stokes line is crossed, A rapidly increases from 0 to $2\pi\mathrm{i}/\epsilon^{1/2}$. From (4.6), we therefore find that the jump in $S^{(N)}$ across the Stokes line is

$$[S^{(N)}]_-^+ = \frac{2\pi\mathrm{i}\Xi}{\epsilon^{1/2}}\mathrm{e}^{-\chi/\epsilon}. \tag{4.17}$$

4.1. *Longitudinal waves*

There are two active contributions to the late-order terms, associated with $\chi_{L1,2}$, which are switched on by the leading-order behaviour. Using (3.13), the associated free-surface behaviour is given by

$$[S^{(N)}_{TOT}]_-^+ = \frac{2\pi\mathrm{i}\chi_x\Phi}{\epsilon^{1/2}}\mathrm{e}^{-\chi_{L1}/\epsilon} + \mathrm{c.c.} \tag{4.18}$$

(recall that χ_{L2} is the complex conjugate of χ_{L1}). The radiation condition implies that there are no waves upstream, so we find that gravity waves of the form given in (4.18) are present on the downstream free surface. Figure 3 illustrates the behaviour of these waves for $\epsilon = 0.15$, $h = 1$. Along the curve $y = 0$, we find that the far-field behaviour is given by

$$\xi_{exp} \sim \sqrt{\frac{h}{8\pi\epsilon x}}\mathrm{e}^{-h/\epsilon}\cos\left(\frac{x}{\epsilon}\right). \tag{4.19}$$

https://doi.org/10.1017/jfm.2013.425 Published online by Cambridge University Press

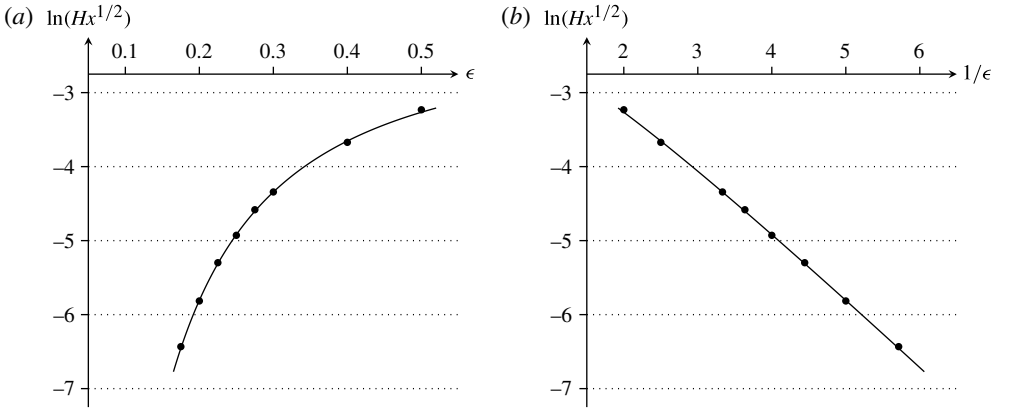


FIGURE 4. Comparison of asymptotic and numerical values for the far-field gravity wave amplitude along $y = 0$, scaled by the strength of the source, for varying values of (*a*) ϵ and (*b*) $1/\epsilon$. The source is fixed at depth $h = 1$. The solid line represents the asymptotic value for the amplitude, given in (4.19), multiplied by $x^{1/2}$ so that it takes a constant value in the far field. The slope of the line in (*b*) is equal to $-h$, which may be seen by noting the value of the singulant in the far field. The circles represent the equivalent value obtained from numerical solutions to the exact problem. The asymptotic results provide an accurate approximation to the exact solution.

We recall from figure 2 that the Stokes line intersects the free surface along the curve $x = 0$. Despite this, we see that the waves appear to be restricted to a wedge behind the source with an angle to the horizontal of approximately the Kelvin angle. Although there are exponentially small waves everywhere in $x > 0$, the exponential is almost constant in the Kelvin wedge, decaying rapidly outside it. This behaviour is illustrated by the contour behaviour in figure 3.

Figure 4 compares the far-field amplitude predicted by the asymptotic analysis along the line $y = 0$ with numerical results. These numerical results were obtained by expressing the solution to (2.7)–(2.9) as an integral which was subsequently evaluated numerically. Details of the numerical procedure are given in appendix B. Specifically, we compare the amplitude of the expression in (4.19), denoted by H, with the numerically calculated solution for a range of values of ϵ. It is clear that the asymptotic results provide an accurate approximation for the exact longitudinal wave behaviour.

5. Subdominant wave switching

In the previous analyses of the Stokes structure of partial differential equations (see Howls, Langman & Olde Daalhuis 2004; Chapman & Mortimer 2005), it was found that Stokes switching may also occur when one exponentially subdominant contribution switches on a further subdominant contribution. Hence, we find that Stokes switching also occurs on curves satisfying $\mathrm{Im}(\chi_{L1}) = \mathrm{Im}(\chi_{T1})$ and $\mathrm{Re}(\chi_{L1}) < \mathrm{Re}(\chi_{T1})$, across which the transverse wave behaviour associated with $\chi_{T1,2}$ is switched on. Along these curves, the same conditions will also be satisfied by χ_{L2} and χ_{T2}, which are the respective complex-conjugate expressions.

To fully illustrate the Stokes behaviour in this problem, and to recover Keller's solution in the limit that $h \to 0$, we examine the behaviour of the Stokes lines

https://doi.org/10.1017/jfm.2013.425 Published online by Cambridge University Press

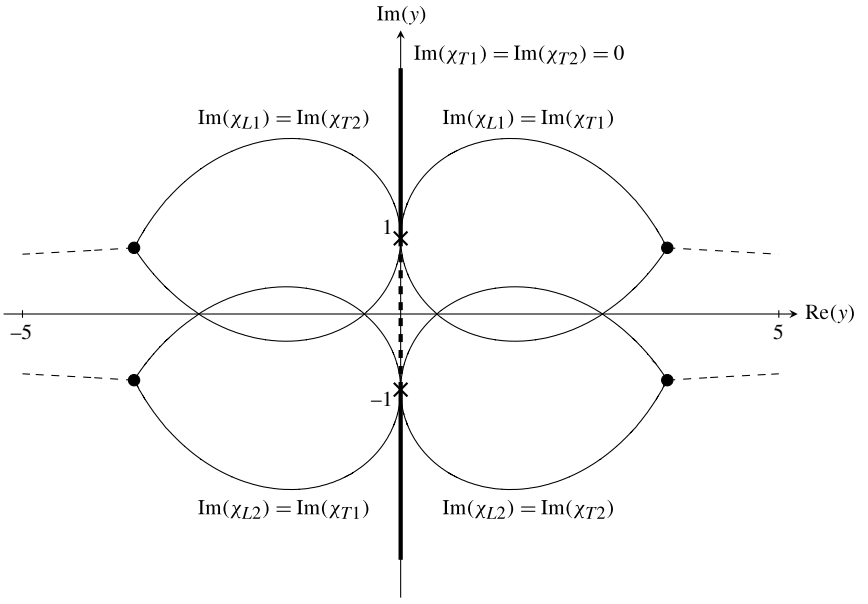


FIGURE 5. Stokes structure for flow over a source of depth $h = 1$, where $x = 10$ and $y \in \mathbb{C}$. Turning points and singularities are represented by circles and crosses respectively. Active Stokes lines are shown as solid black curves, while inactive Stokes lines are shown as dashed black curves. Stokes lines that follow the imaginary axis are shown in bold for clarity. The switching behaviour associated with these Stokes lines is shown in figure 6.

for $y \in \mathbb{C}$ and fixed x in figure 5. The solution contains four turning points, or caustics. In the neighbourhood of each caustic, the interaction of the singulant terms produces the local Stokes structure of an Airy function (discussed in Chapman *et al.* 1999 and elsewhere), with three anti-Stokes lines and three Stokes lines (one of which is inactive) intersecting. The pattern of Stokes and anti-Stokes lines originating at a single turning point is illustrated in figure 6.

In figure 6, we show which of the late-order contributions is present in each region of the analytically continued free surface. Importantly, we see that the contribution associated with χ_{L1} is present over the entirety of the physical free surface, while the contribution associated with χ_{T1} is restricted to a region of finite width, between the two active Stokes lines.

Figure 7 illustrates the location of the Stokes lines on the physical free surface for a range of values of h. The longitudinal wave contribution is present in the entire downstream region, while the transverse wave contribution is restricted to two separate wedge-like regions on either side of $y = 0$. As h increases, the waves switch on further downstream, while as h tends to zero, the downstream wave region tends to the Kelvin wedge. Each contribution is exponentially small, having $\mathrm{Re}(\chi) > 0$ over the entire active region, and the transverse waves are exponentially subdominant to the longitudinal waves. However, both waves become algebraic in the limit $h \to 0$, which we will examine in § 6.1.

In figures 8(*a*) and 8(*b*) we show the phase of the downstream free-surface waves for $h = 1$ associated with $\chi_{L1,2}$ and $\chi_{T1,2}$ respectively. Here we see the reason for the nomenclature: the longitudinal waves are primarily moving in the direction of the x-axis, while the transverse waves are moving outwards from the x-axis.

https://doi.org/10.1017/jfm.2013.425 Published online by Cambridge University Press

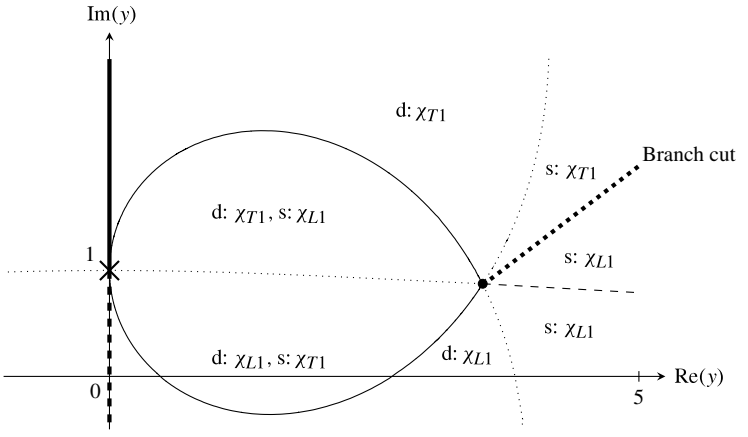


FIGURE 6. Stokes switching in the first quadrant about a caustic. Active Stokes lines are shown as solid black curves, while the inactive Stokes line is shown as a dashed curve. There is a Stokes line present on the imaginary axis, shown as a thick black curve. The thin dotted lines indicate anti-Stokes lines, and the thick dotted line represents a branch cut across which the labels of χ_L and χ_T switch. In the neighbourhood of the caustic, the singulant behaves like that of an Airy function. In each region, the active singulant contributions are indicated, and allocated the letter 's' or 'd' to denote either subdominance or dominance with respect to the other contribution. The real axis represents the free surface, and we see that the contribution associated with χ_{L1} is active on the entire real axis, while that associated with χ_{T1} is restricted to a finite region.

6. Varying the source depth

We show in figure 9 the real part of $\chi_{L1,2}$ along the cross-section $x = 3$ for various values of h. We see that $\mathrm{Re}(\chi_{L1,2})$ increases as h is increased. Consequently, the amplitude of the longitudinal waves on the free surface decreases exponentially as the depth of the source increases, in keeping with (4.19). As $h \to 0$, $\mathrm{Re}(\chi_{L1,2})$ becomes zero within the Kelvin wedge, corresponding to the waves there ceasing to be exponentially small. We see that even for non-zero h, $\mathrm{Re}(\chi_{L1,2})$ is roughly constant within the wedge region, while increasing outside it, explaining the wedge-like behaviour seen in figure 3.

The effect of the source depth on the location of the Stokes lines across which the transverse waves are switched on was exhibited in figure 7. There, we noted that as the depth increases, the transverse waves are switched on further downstream, and that this switching region tends to the Kelvin wedge in the limit that $h \to 0$. The effect of varying the source depth on the transverse-wave amplitude is more complicated than the longitudinal case, as seen in figure 10; however, it is always true that $\mathrm{Re}(\chi_{T1,2}) > \mathrm{Re}(\chi_{L1,2})$ in regions where transverse waves are present on the free surface, and therefore that the transverse waves will always be exponentially dominated by longitudinal waves, with the exception of the zero-depth case.

6.1. *Zero source depth*

The problem of linearized low-Froude-number flow with a source positioned on the surface was considered in Keller (1979). That study showed that the free surface will contain both longitudinal and transverse waves of algebraic order in a downstream

https://doi.org/10.1017/jfm.2013.425 Published online by Cambridge University Press

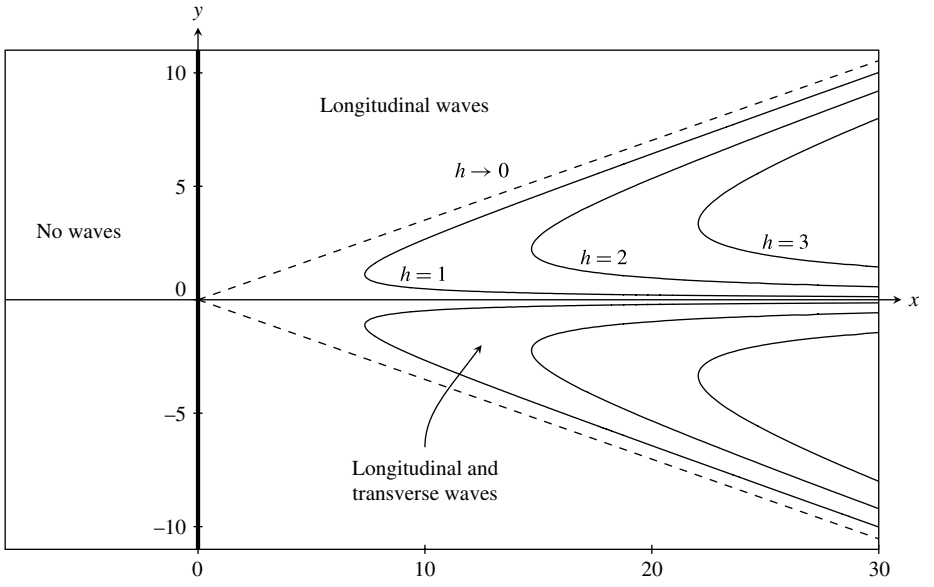


FIGURE 7. Stokes lines on the free surface of the flow. The bold curve represents the Stokes line across which downstream longitudinal waves associated with $\chi_{L1,2}$ are switched on. The thin curves represent the Stokes lines across which downstream transverse waves associated with $\chi_{T1,2}$ are switched on, for a range of values of h. As h tends to zero, the region in which transverse waves are present tends to a wedge, as predicted by Keller (1979). As h increases, the waves are switched on further downstream.

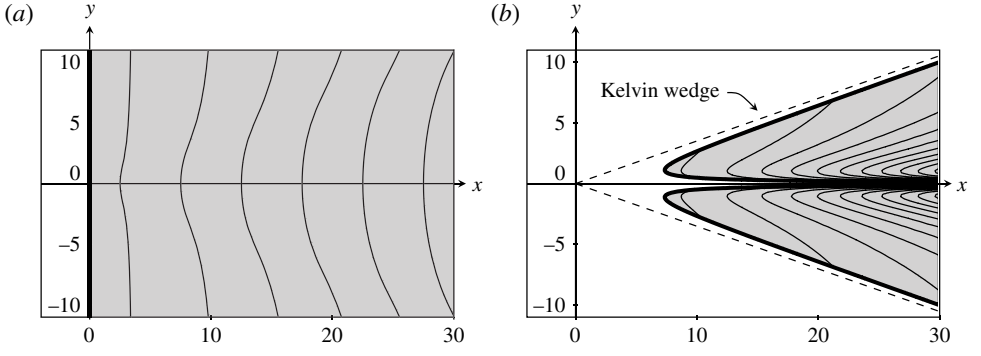


FIGURE 8. Equal phase lines for the free-surface behaviour associated with (*a*) $\chi_{L1,2}$ and (*b*) $\chi_{T1,2}$ for $h = 1$, represented as thin black curves. Each wave contribution is switched on across Stokes lines, shown as thick black curves. The contributions are active on the shaded region of the free surface. For reference, the Kelvin wedge is illustrated as a dashed curve. It is clear that the wave behaviour illustrated in (*a*) takes the form of longitudinal waves, while in (*b*) takes the form of transverse waves.

wedge defined by $|x/y| > 2\sqrt{2}$. This implies that the singulant will be purely imaginary in this region when $h = 0$. Solving (3.7) and setting $h = 0$ in the boundary conditions (3.8), giving

$$x_0 = 0, \quad y_0 = 0, \quad \chi_0 = 0, \tag{6.1}$$

https://doi.org/10.1017/jfm.2013.425 Published online by Cambridge University Press

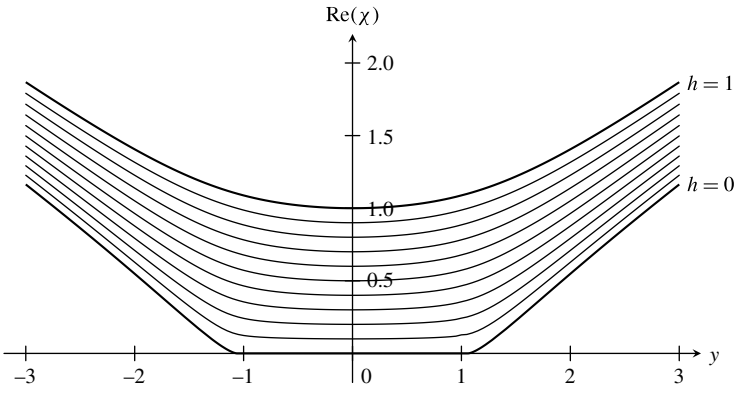


FIGURE 9. Cross-section of $\mathrm{Re}(\chi_{L1,2})$ along the line $x = 3$ for $h = 0, 0.1, \ldots, 1$. As the depth of the source increases, the real part the singulant also decreases, and hence the waves become exponentially smaller in amplitude. At $h = 0$, the singulant may be divided into a purely imaginary part in a finite region about $y = 0$, and complex parts that lie outside this region. This is consistent with previous work on Kelvin waves (such as Kelvin 1887; Keller 1979).

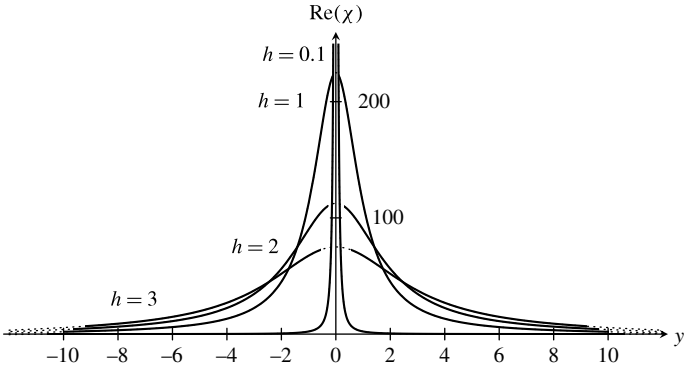


FIGURE 10. Cross-section of $\mathrm{Re}(\chi_{T1,2})$ along the line $x = 30$ for $h = 0.1, 1, 2, 3$, where solid lines indicate that the transverse waves are switched on, and dotted lines indicate that they are not. As the depth of the source increases, the real part the singulant flattens, and hence the waves become larger in the central region, but smaller further from the centre. As $h \to 0$, the width of the central peak tends to zero, and the height tends to infinity. Aside from this peak, $\mathrm{Re}(\chi_{T1,2})$ tends to zero within the Kelvin wedge, and hence the transverse waves are algebraically small in this limit. We see that for all values of h, $\mathrm{Re}(\chi) > 0$ in the regions where transverse waves are present, although this is not true in regions where they are not present.

gives the singulant as

$$\chi = \frac{\alpha^3 x}{2\alpha^2 + 1}, \tag{6.2}$$

where α is a solution to

$$4y^2\alpha^4 + \left(x^2 + 4y^2\right)\alpha^2 + \left(x^2 + y^2\right) = 0. \tag{6.3}$$

https://doi.org/10.1017/jfm.2013.425 Published online by Cambridge University Press

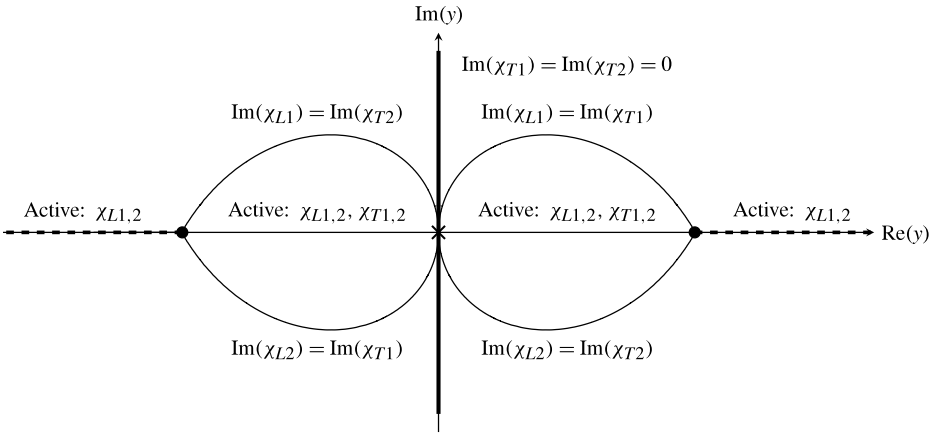


FIGURE 11. Stokes structure for flow over a source with $h = 0$, for $x > 0$ and $y \in \mathbb{C}$. The turning point and singularity are represented by a circle and cross respectively. Stokes lines which cause switching behaviour are shown as solid black curves, while inactive Stokes lines are shown as dashed black curves. Stokes lines following the axes are illustrated in bold for clarity. The turning point is located at $y = 2\sqrt{2}$. The contributions in each region of the physical free surface are indicated directly.

In this case, α has purely imaginary solutions for $|x/y| > 2\sqrt{2}$, and therefore χ is also purely imaginary in this region as required. Noting that the corresponding free-surface contributions are only switched on in the downstream wave region, this is therefore consistent with the results of Keller (1979). In figure 11, we illustrate the behaviour of each of the four singulant contributions at $h = 0$, for a fixed value of $x > 0$. As noted, all four contributions are purely imaginary within the range $|x/y| > 2\sqrt{2}$, which implies that any resultant waves present on the free surface within this wedge are of algebraic order. This is confirmed by considering the $h \to 0$ limit in figures 9 and 10 for longitudinal and transverse waves respectively.

Figure 11 illustrates the full Stokes structure of the problem for fixed $x > 0$, with y permitted to take complex values. In comparing this structure to that illustrated in figure 6, we see that the turning points have coalesced on the physical free surface. In order for this behaviour to be consistent with the $h > 0$ case, we determine that the contribution associated with $\chi_{T1,2}$ is present between the two turning points, and hence is restricted to the wedge on the free surface defined by $|x/y| > 2\sqrt{2}$. This is consistent with the limiting behaviour of the Stokes lines demonstrated in figure 7.

The contribution associated with $\chi_{L1,2}$, however, is present for all $x > 0$, switching in the same manner as the corresponding contributions for $h > 0$. The resultant waves are of algebraic order within the region defined by $|x/y| > 2\sqrt{2}$, but exponentially small outside of this wedge. The resultant downstream wave regions are illustrated in figure 12.

These results are consistent with those of Ursell (1960), who showed that the wave behaviour near the critical angle took the form of an Airy function. This may be seen in figure 11, showing that the turning points intersect the free surface on the critical angle when $h = 0$.

https://doi.org/10.1017/jfm.2013.425 Published online by Cambridge University Press

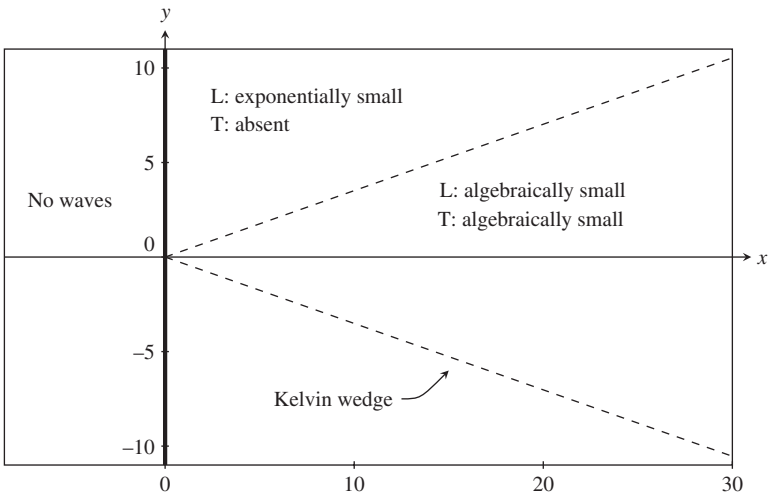


FIGURE 12. Free-surface behaviour with $h = 0$. The Stokes line and caustics are represented as bold curves and dashed curves respectively. There are no upstream waves present, and the behaviour of the downstream longitudinal and transverse waves is described directly in the figure. The caustic is located on the edge of the Kelvin wedge, and therefore follows $|x/y| = 2\sqrt{2}$.

7. Discussion and conclusions

In this investigation, we calculated the behaviour of steady waves on the free surface of flow over a point source in three dimensions. We considered the source to be weak, and therefore linearized the problem about the undisturbed solution. We subsequently applied exponential asymptotic techniques in order to determine the behaviour of the resultant free-surface waves, finding that Stokes switching caused by the interaction between exponentially subdominant free-surface contributions plays an important role in the wave behaviour.

The flow contains longitudinal waves that are switched on across the Stokes line following $x = 0$, and are present in the entire right-half-plane. The behaviour of these waves may be seen in figure 3. While the longitudinal wave contribution is present in the entire right-half-plane, the amplitude of the waves decays away from the x-axis so that the visible waves appear to be restricted to a wedge.

The far-field amplitude of these longitudinal waves was compared to numerical solutions to the linearized equations in figure 4. The numerical results were obtained by formulating the solution to the linearized system as an integral equation using methods similar to those given in Havelock (1932) and Noblesse (1981), and evaluating the integral numerically. The comparison showed good agreement between the asymptotic and numerical results.

By comparing the singulants associated with the transverse wave and longitudinal wave contributions, we found that transverse waves are switched on across Stokes lines containing approximately wedge-shaped regions on either side of the curve $y = 0$, as seen in figure 7. While we did not compute the prefactor associated with this behaviour, knowledge of the singulant is sufficient to determine the phase of the waves produced by this contribution. Hence, we have determined that, in the steady-state

https://doi.org/10.1017/jfm.2013.425 Published online by Cambridge University Press

problem, the leading-order behaviour switches on the downstream longitudinal waves, and these waves switch on a subdominant downstream transverse wavetrain.

Finally, we showed that, in the limit $h \to 0$, this analysis agrees with the low-Froude-number behaviour found by Keller (1979) when the singularity is located on the free surface. In this case, the longitudinal waves are only algebraically small (having $\mathrm{Re}(\chi) = 0$) within a downstream wedge bounded by the curves $|x/y| = 2\sqrt{2}$, and exponentially small outside of this wedge. Furthermore, the Kelvin wedge also contains algebraically small transverse wave behaviour which is not present outside of the wedge. This is caused by the existence of Airy-type behaviour along the edge of the wedge region, which was noted by Ursell (1960).

Appendix A. Inner problem

To solve the inner problem, we first consider the behaviour of χ_{L1} near the singularity at $x^2 + y^2 + (z+h)^2 = 0$, which takes the form

$$\chi_{L1} \sim \frac{h}{2x^2}\left(x^2 + y^2 + (z+h)^2\right). \tag{A 1}$$

In the prefactor (3.19), we see that the unknown coefficient is a function of s. From (3.9), it follows that $s \sim x$ near the singularity at $t = 0$. Hence, we define a system of inner coordinates given by

$$\epsilon\sigma_1 = \frac{h}{2x^2}(x^2 + y^2 + (z+h)^2), \quad \epsilon\sigma_2 = \frac{h}{2x^2}(x^2 + y^2 + (z-h)^2), \quad \lambda = x. \tag{A 2}$$

To leading-order in ϵ, the linearized governing equation (2.7) becomes (omitting the bars)

$$\sigma_1\phi_{\sigma_1\sigma_1} - \sigma_2\phi_{\sigma_2\sigma_2} + \lambda\phi_{\lambda\sigma_2} - \lambda\phi_{\lambda\sigma_1} = 0, \tag{A 3}$$

where terms containing derivatives with respect to both σ_1 and σ_2 were disregarded due to the eventual form of the inner expansion, (A 7). Similarly, to leading-order in ϵ, the boundary conditions (2.8)–(2.9) become

$$h\phi_{\sigma_1} - h\phi_{\sigma_2} - \lambda\xi_{\sigma_1} - \lambda\xi_{\sigma_2} = 0 \quad \text{on } \sigma_1 = \sigma_2, \tag{A 4}$$

$$h\phi_{\sigma_1} + h\phi_{\sigma_2} + \lambda\xi = 0 \quad \text{on } \sigma_1 = \sigma_2. \tag{A 5}$$

Finally, by expressing the leading-order behaviour (2.16) in terms of the local variables, we find that near the singularity on the complexified free surface

$$\phi^{(0)} \sim \frac{h^{1/2}}{4\sqrt{2}\pi\epsilon^{1/2}\lambda^{1/2}}\frac{1}{\sigma_1^{1/2}} + \frac{h^{1/2}}{4\sqrt{2}\pi\epsilon^{1/2}\lambda^{1/2}}\frac{1}{\sigma_2^{1/2}}, \quad \xi^{(0)} = 0. \tag{A 6}$$

We now define the series expansion near the singularity on the complexified free surface as

$$\phi \sim \sum_{n=0}^{\infty}\left[\frac{a_n(\lambda)\Gamma(n+1/2)}{\sigma_1^{n+1/2}} + \frac{b_n(\lambda)\Gamma(n+1/2)}{\sigma_2^{n+1/2}}\right], \quad \xi \sim \sum_{n=0}^{\infty}\left[\frac{2c_n(\lambda)\Gamma(n+1/2)}{\sigma_1^{n+1/2}}\right], \tag{A 7}$$

where the latter expression is only valid on the free surface itself, on which $\sigma_1 = \sigma_2$. The factor of two is included for subsequent algebraic convenience, and has no effect

https://doi.org/10.1017/jfm.2013.425 Published online by Cambridge University Press

on the solution to the problem as c_n is unknown at this stage. From (A 6), we have

$$a_0(\lambda) = \frac{h^{1/2}}{4\sqrt{2}\pi\lambda^{1/2}}, \quad b_0(\lambda) = \frac{h^{1/2}}{4\sqrt{2}\pi\lambda^{1/2}}, \quad c_0 = 0. \tag{A 8}$$

We are interested in the behaviour of the terms on the complexified free surface in the neighbourhood of the singularity at $x^2 + y^2 + h^2 = 0$. Consequently, we apply the series expression to (A 4) on the surface (defined by $\sigma_1 = \sigma_2$) and match in the limit that σ_1 (and therefore σ_2) tend to zero, giving

$$h(a_n - b_n) - 2\lambda c_n = 0, \quad n \geqslant 0. \tag{A 9}$$

Applying the series expansion to (A 5) and matching in the same limit gives

$$-h(n + 1/2)(a_n + b_n) + 2\lambda c_{n+1} = 0, \quad n \geqslant 0. \tag{A 10}$$

We are interested in the behaviour on the complexified free surface; however, restricting the domain in this fashion means that it is impossible to distinguish between the contributions from the series in σ_1 and the series in σ_2. However, we see that the two contributions have equal magnitude in (A 6). As the singular behaviour of the problem is preserved in all higher-orders (see Dingle 1973), we conclude that this must be true of the contributions at all subsequent orders. We therefore specify that $|a_n| = |b_n|$ in order to maintain consistency with the leading-order behaviour. This may only be accomplished if we divide the two equations given in (A 9)–(A 10) into four equations such that

$$ha_n - \lambda c_n = 0, \quad -h(n + 1/2)a_n + \lambda c_{n+1} = 0, \tag{A 11a}$$

$$-hb_n - \lambda c_n = 0, \quad -h(n + 1/2)b_n + \lambda c_{n+1} = 0. \tag{A 11b}$$

We will consider only the first two of these equations, noting that the remaining equations imply that $b_n = (-1)^n a_n$. Eliminating c_n from this system gives

$$a_{n+1} = (n + 1/2)a_n = \frac{a_0\Gamma(n + 1/2)}{\Gamma(1/2)}. \tag{A 12}$$

Hence, using the expression for a_0 given in (A 8), we may match the local series expression given in (A 7) with the prefactor given in (3.19). Noting that λ is the local expression for s in the outer solution, we find that

$$\Phi(s, 0) = \frac{h^{1/2}}{4\pi s^{1/2}\sqrt{2\pi}}. \tag{A 13}$$

Hence, we are able to completely describe the late-order behaviour of terms in (2.11).

Appendix B. Numerical calculations

In order to verify the asymptotic results obtained in § 4, we will compare them to numerical solutions to the system described in (2.7)–(2.10). These solutions will be obtained by computing the solution to a double integral formulation for the free-surface behaviour. We will formulate the integral expression here, but we note that many similar integral expressions have been found in previous work, such as Noblesse (1981). We set

$$\phi = \frac{1}{4\pi\sqrt{x^2 + y^2 + (z - h)^2}} + \frac{1}{4\pi\sqrt{x^2 + y^2 + (z + h)^2}} + \hat{\phi}. \tag{B 1}$$

https://doi.org/10.1017/jfm.2013.425 Published online by Cambridge University Press

Then

$$\nabla^2\hat{\phi} = 0, \tag{B 2}$$

with boundary conditions given by

$$\epsilon\hat{\phi}_x + \xi = -\epsilon\left[\frac{1}{2\pi\sqrt{x^2+y^2+h^2}}\right]_x, \quad z = 0, \tag{B 3}$$

$$\hat{\phi}_z - \xi_x = 0, \quad z = 0. \tag{B 4}$$

The far-field conditions determine that $\hat{\phi} \to 0$ far from the source. Taking the Fourier transform of (B 2) with respect to x and y (with the resultant expression given in terms of the Fourier variables k and l respectively) gives

$$\overline{\overline{\phi}}_{zz} - \rho^2\overline{\overline{\phi}} = 0, \tag{B 5}$$

where $\rho = \sqrt{k^2+l^2}$. Noting that the solution must decay in the limit that $z \to -\infty$, this differential equation may be solved to give

$$\overline{\overline{\phi}} = A(k,l)\mathrm{e}^{\rho z}. \tag{B 6}$$

Taking the Fourier transform of the boundary conditions (B 3)–(B 4) gives

$$\epsilon\mathrm{i}k\overline{\overline{\phi}} + \overline{\overline{\xi}} = -\mathrm{i}k\epsilon\,\mathscr{F}_{xy}\left[\frac{1}{2\pi\sqrt{x^2+y^2+h^2}}\right], \quad z = 0, \tag{B 7}$$

$$\overline{\overline{\phi}}_z - \mathrm{i}k\overline{\overline{\xi}} = 0, \quad z = 0. \tag{B 8}$$

Using the expression given in (B 6), this becomes

$$\epsilon\mathrm{i}kA + \overline{\overline{\xi}} = -\mathrm{i}k\epsilon\,\mathscr{F}_{xy}\left[\frac{1}{2\pi\sqrt{x^2+y^2+h^2}}\right], \tag{B 9}$$

$$\rho A - \mathrm{i}k\overline{\overline{\xi}} = 0, \tag{B 10}$$

where

$$\begin{aligned}\mathscr{F}_{xy}\left[\frac{1}{2\pi\sqrt{x^2+y^2+h^2}}\right] &= \int_0^\infty\int_0^{2\pi}\frac{r}{2\pi\sqrt{r^2+h^2}}\mathrm{e}^{-\mathrm{i}r\rho\cos(\theta-\phi)}\,\mathrm{d}\theta\,\mathrm{d}r,\\ &= \int_0^\infty\frac{rJ_0(\rho r)}{\sqrt{r^2+h^2}}\,\mathrm{d}r,\\ &= \frac{\mathrm{e}^{-\rho h}}{\rho}.\end{aligned} \tag{B 11}$$

Eliminating A from (B 9)–(B 10) gives

$$\overline{\overline{\xi}} = \frac{\mathrm{i}k\epsilon\mathrm{e}^{-\rho h}}{\rho - \epsilon k^2}. \tag{B 12}$$

Taking the inverse Fourier transform, we find that

$$\xi = \frac{1}{4\pi^2}\int_{-\infty}^{\infty}\int_{-\infty}^{\infty}\frac{\mathrm{i}k\epsilon\mathrm{e}^{-\rho h}}{\rho - \epsilon k^2}\mathrm{e}^{\mathrm{i}kx+\mathrm{i}ly}\,\mathrm{d}k\,\mathrm{d}l. \tag{B 13}$$

https://doi.org/10.1017/jfm.2013.425 Published online by Cambridge University Press

We note that this integral is singular along the curve $\rho = \epsilon k^2$. In order to evaluate this integral numerically, we would prefer this curve to follow a straight line. Hence, we first transform into polar coordinates, giving

$$\xi = \frac{1}{4\pi^2}\int_0^{\infty}\int_0^{2\pi} \frac{\mathrm{i}\rho\cos\phi\,\epsilon \mathrm{e}^{-\rho h}}{1-\epsilon\rho\cos^2\phi}\mathrm{e}^{\mathrm{i}r\rho\cos(\theta-\phi)}\,\mathrm{d}\phi\,\mathrm{d}\rho. \tag{B 14}$$

Setting $\rho = u/\cos^2\phi$, we finally obtain

$$\xi = \frac{1}{4\pi^2}\int_0^{2\pi}\!\!\!\!\!\!-\int_0^{\infty} \frac{\mathrm{i}u\epsilon}{(1-\epsilon u)\cos^3\phi}\exp\left(\frac{\mathrm{i}ur\cos(\theta-\phi)-uh}{\cos^2\phi}\right)\mathrm{d}u\,\mathrm{d}\phi, \tag{B 15}$$

where we see that the integrand is singular along $u = 1/\epsilon$ and hence that the inner integral may be treated as a Cauchy principal value integral about this point, which we have indicated explicitly. Additionally, we note that there are removable singularities along $\phi = \pi/2$ and $\phi = 3\pi/2$, which do not cause any numerical difficulties.

This integral is substantially more complicated than the forms given in (B 13)–(B 14). However, the fact that the integrand is singular along a straight line ensures that it is more simple to solve using standard numerical integration in two dimensions.

In order to evaluate (B 15) numerically for given values of h and ϵ, we truncate the integral domain in the u-direction and split it into two regions, given by

$$D1 = \{(u,\phi) : u \in (0, 1/\epsilon - \Delta),\ \phi \in (0, 2\pi)\}, \tag{B 16a}$$

$$D2 = \{(u,\phi) : u \in (1/\epsilon + \Delta, u_\infty),\ \phi \in (0, 2\pi)\}, \tag{B 16b}$$

where Δ is a small constant used to approximate the Cauchy principal value integral, and u_∞ is the truncation point. Typical values used in this investigation are $\Delta = 1\times10^{-5}$ and $u_\infty = 50$. On each domain, we evaluate the two-dimensional integral numerically using the inbuilt MATLAB integrator, which uses two-dimensional quadrature techniques.

REFERENCES

ABRAMOWITZ, M. & STEGUN, I. 1972 *Handbook of Mathematical Functions with Formulas, Graphs, and Mathematical Tables*. Dover.

AKYLAS, T. R. 1987 Unsteady and nonlinear effects near the cusp lines of the Kelvin ship-wave pattern. *J. Fluid Mech.* **175**, 333–342.

BABA, E. 1976 Wave resistance of ships in low speed. *Mitusubishi Tech. Bull.* **109**, 1–20.

BERRY, M. V. 1988 Stokes phenomenon; smoothing a Victorian discontinuity. *Pub. Math. de L'IHÉS* **68**, 211–221.

BERRY, M. V. 1991 Asymptotics, superasymptotics, hyperasymptotics. In *Asymptotics Beyond All Orders* (ed. H. Segur, S. Tanveer & H. Levine), pp. 1–14. Plenum.

BERRY, M. V. & HOWLS, C. J. 1990 Hyperasymptotics. *Proc. R. Soc. Lond.* A **430** (1880), 653–668.

BOYD, J. P. 1998 *Weakly Non-local Solitary Waves and Beyond-All-Orders Asymptotics: Generalized Solitons and Hyperasymptotic Perturbation Theory*. Mathematics and Its Applications, vol. 442, Kluwer.

BOYD, J. P. 1999 The devils invention: Asymptotic, superasymptotic and hyperasymptotic series. *Acta Appl. Maths* **56** (1), 1–98.

BOYD, J. P. 2005 Hyperasymptotics and the linear boundary layer problem: why asymptotic series diverge. *SIAM Rev.* **47** (3), 553–575.

https://doi.org/10.1017/jfm.2013.425 Published online by Cambridge University Press

CHAPMAN, S. J., KING, J. R., OCKENDON, J. R. & ADAMS, K. L. 1978 Exponential asymptotics and Stokes lines in nonlinear ordinary differential equations. *Proc. R. Soc. Lond.* A **454**, 2733–2755.

CHAPMAN, S. J., LAWRY, J. M. H. & TEW, R. H. 1999 On the theory of complex rays. *SIAM Rev.* **41** (3), 417–509.

CHAPMAN, S. J. & MORTIMER, D. B. 2005 Exponential asymptotics and Stokes lines in a partial differential equation. *Proc. R. Soc. Lond.* A **461**, 2385–2421.

CHAPMAN, S. J. & VANDEN-BROECK, J.-M. 2002 Exponential asymptotics and capillary waves. *SIAM J. Appl. Maths* **62** (6), 1872–1898.

CHAPMAN, S. J. & VANDEN-BROECK, J.-M. 2006 Exponential asymptotics and gravity waves. *J. Fluid Mech.* **567**, 299–326.

COSTIN, O. & KRUSKAL, M. D. 1996 Optimal uniform estimates and rigourous asymptotics beyond all orders for a class of ordinary differential equations. *Proc. R. Soc. Lond.* A **452** (1948), 1057–1085.

COSTIN, O. & KRUSKAL, M. D. 1999 On optimal truncation of divergent series solutions of nonlinear differential systems. *Proc. R. Soc. Lond.* A **455** (1985), 1931–1956.

DAGAN, G. & TULIN, M. P. 1972 Two-dimensional free-surface gravity flow past blunt bodies. *J. Fluid Mech.* **51** (3), 529–543.

DINGLE, R. B. 1973 *Asymptotic Expansions: Their Derivation and Interpretation*. Academic.

FORBES, L. K. & SCHWARTZ, L. W. 1982 Free surface flow over a semi-circular obstruction. *J. Fluid Mech.* **114**, 299–314.

GRIMSHAW, R. 2011 Exponential asymptotics and generalized solitary waves. In *Asymptotic Methods in Fluid Mechanics: Survey and Recent Advances* (ed. H. Steinrück, F. Pfeiffer, F. G. Rammerstorfer, J. Salençon, B. Schrefler & P. Serafini), CISM Courses and Lectures, vol. 523, pp. 71–120. Springer.

GRIMSHAW, R. & JOSHI, N. 1995 Weakly non-local solitary waves in a singularly perturbed Korteweg-de Vries equation. *SIAM J. Appl. Maths* **55** (1), 124–135.

HAVELOCK, T. H. 1917 Some cases of wave motion due to a submerged obstacle. *Proc. R. Soc. Lond.* A **93** (654), 520–532.

HAVELOCK, T. H. 1919 Wave resistance: some cases of three-dimensional fluid motion. *Proc. R. Soc. Lond.* A **95** (670), 354–365.

HAVELOCK, T. H. 1931 The wave resistance of a spheroid. *Proc. R. Soc. Lond.* A **131** (817), 275–285.

HAVELOCK, T. H. 1932 The theory of wave resistance. *Proc. R. Soc. Lond.* A **138** (835), 339–348.

HAVELOCK, T. H. 1949 The wave resistance of a cylinder started from rest. *Q. J. Mech. Appl. Maths* **2** (3), 325–334.

HOWLS, C. J., LANGMAN, P. J. & OLDE DAALHUIS, A. B. 2004 On the higher-order Stokes phenomenon. *Proc. R. Soc. Lond.* A **460** (2121), 2285–2303.

JONES, D. S. 1997 *Introduction to Asymptotics: a Treatment Using Nonstandard Analysis*, p. 160. World Scientific.

KELLER, J. B. 1979 The ray theory of ship waves and the class of streamlined ships. *J. Fluid Mech.* **91** (3), 465–488.

KELLER, J. B. & WARD, M. J. 1996 Asymptotics beyond all orders for a low Reynolds number flow. *J. Engng Maths* **30** (1–2), 253–265.

KELVIN, LORD 1887 On ship waves. *Proc. Inst. Mech. Engrs* **3**, 409–434.

LAMB, H. 1879 *Hydrodynamics*. Cambridge University Press.

LIU, M. & TAO, M. 2001 Transient ship waves on an incompressible fluid of infinite depth. *Phys. Fluids* **13**, 3610–3623.

LUNDE, J. K. 1951 On the linearized theory of wave resistance for displacement ships in steady and accelerated motion. *Trans.-Soc. Nav. Archit. Mar. Eng* **59**, 25–76.

LUSTRI, C. J., MCCUE, S. W. & BINDER, B. J. 2012 Free surface flow past topography: a beyond-all-orders approach. *Eur. J. Appl. Maths* **23** (4), 441–467.

LUSTRI, C. J., MCCUE, S. W. & CHAPMAN, S. J. 2013 Exponential asymptotics of free surface flow due to a line source. *IMA J. Appl. Maths* **78** (4), 697–713.

https://doi.org/10.1017/jfm.2013.425 Published online by Cambridge University Press

MARUO, H. & SUZUKI, K. 1977 Wave resistance of a ship of finite beam predicted by the low speed theory. *J. Soc. Nav. Arch. Japan* **142**, 1–7.

MICHELL, J. H. 1898 The wave-resistance of a ship. *Phil. Mag.* **45** (5), 106–123.

NOBLESSE, F. 1981 Alternative integral representations for the Green function of the theory of ship wave resistance. *J. Engng Maths* **15** (4), 241–265.

NOBLESSE, F. 1982 The Green function in the theory of radiation and diffraction of regular water waves by a body. *J. Engng Maths* **16**, 137–169.

OCKENDON, J. R., HOWISON, S., LACEY, A. & MOVCHAN, A. 1999 *Applied Partial Differential Equations*. Oxford University Press.

OCKENDON, J. R. & WILMOTT, P. 1986 Matching and singularity distributions in inviscid flow. *IMA J. Appl. Maths* **37** (3), 199–211.

OGILVIE, T. F. 1968 Wave resistance: the low speed limit. In *Tech. Rep*. Ann Arbor, MI, Michigan University.

OLDE DAALHUIS, A. B. 1998 Hyperasymptotic solutions of higher-order linear differential equations with a singularity of rank one. *Proc. R. Soc. Lond.* A **454** (1968), 1–29.

OLDE DAALHUIS, A. B., CHAPMAN, S. J., KING, J. R., OCKENDON, J. R. & TEW, R. H. 1995 Stokes phenomenon and matched asymptotic expansions. *SIAM J. Appl. Maths* **55** (6), 1469–1483.

PARIS, R. B. & WOOD, A. D. 1995 Stokes phenomenon demystified. *IMA Bull.* **31**, 21–28.

PEREGRINE, D. H. 1972 A line source beneath a free surface. In *Mathematics Research Center Technical Summary Report 1248*. University of Wisconsin.

PETERS, A. S. 1949 A new treatment of the ship wave problem. *Commun. Pure Appl. Maths* **2** (2–3), 123–148.

SEGUR, H., TANVEER, S. & LEVINE, H. (Eds) 1991 *Asymptotics Beyond All Orders*. Plenum.

STOKES, G. G. 1864 On the discontinuity of arbitrary constants which appear in divergent developments. *Trans. Camb. Phil. Soc.* **10**, 106–128.

TRINH, P. H. 2011 Exponential asymptotics and Stokes line smoothing for generalized solitary waves. In *Asymptotic Methods in Fluid Mechanics: Survey and Recent Advances* (ed. H. Steinrück, F. Pfeiffer, F. G. Rammerstorfer, J. Salençon, B. Schrefler & P. Serafini), CISM Courses and Lectures, vol. 523, pp. 121–126. Springer.

TRINH, P. H. & CHAPMAN, S. J. 2013*a* New gravity-capillary waves at low speeds. Part 1. Linear geometries. *J. Fluid Mech.* **724**, 367–391.

TRINH, P. H. & CHAPMAN, S. J. 2013*b* New gravity-capillary waves at low speeds. Part 2. Nonlinear geometries. *J. Fluid Mech.* **724**, 392–424.

TRINH, P. H., CHAPMAN, S. J. & VANDEN-BROECK, J.-M. 2011 Do waveless ships exist? Results for single-cornered hulls. *J. Fluid Mech.* **685**, 413–439.

URSELL, F. 1960 On Kelvin's ship-wave pattern. *J. Fluid Mech.* **8**, 418–431.

VANDEN-BROECK, J.-M., SCHWARTZ, L. W. & TUCK, E. O. 1978 Divergent low-Froude number series expansion of nonlinear free-surface flow problems. *Proc. R. Soc. Lond.* A **361** (1705), 207–224.

WARD, M. J. & KROPINSKI, M.-C. 2011 Asymptotic methods for pde problems in fluid mechanics and related systems with strong localized perturbations in two-dimensional domains. In *Asymptotic Methods in Fluid Mechanics: Survey and Recent Advances* (ed. H. Steinrück, F. Pfeiffer, F. G. Rammerstorfer, J. Salençon, B. Schrefler & P. Serafini), CISM Courses and Lectures, vol. 523, pp. 23–70. Springer.

WEHAUSEN, J. V. & LAITONE, E. V. 1960 *Surface Waves*. Springer.

https://doi.org/10.1017/jfm.2013.425 Published online by Cambridge University Press